Journal of Applied Polymer Science

Relationship between microstructure of lamellar graphene sheets and properties of polyimide/graphene nanocomposites film under different imidization stages

Xin Ding,[1] Xian Zhang,[1] Chao Bao,[1] Su Tan,[1] Kang Zheng,[1] Lin Chen,[1] Hui Zhang,[2] Xingyou Tian[1]
[1]Chinese Academy of Sciences, Institute of Applied Technology, Hefei institutes of Physical Science, Hefei 230088, People's Republic of China
[2]School of Physics and Materials Science, Anhui University, Hefei 230039, People's Republic of China
Correspondence to: X. Zhang (E-mail: xzhang@issp.ac.cn)

ABSTRACT: Herein, polyimide/graphene sheets (PI/GS) nanocomposite films with different GS distribution structures have been successfully obtained by controlling the imidization degrees, and the effect of the lamellar structure on the properties of PI film has been investigated. The results show that GS are gradually parallel to the surface of PI nanocomposite film with the increase of the imidization temperature, and 150 °C is the critical temperature, where the imidization rate is the fastest and the lamellar structure begins to form. Furthermore, with the drying temperature increasing, the corresponding thermal, electrical and mechanical properties of PI/GS nanocomposite films are significantly improved compared with that of pure PI films, which are ascribed to both the higher imidization degree and the lamellar GS structure. It is noteworthy that the formation process of the lamellar structure at different imidization stages can be directly observed by scanning electron microscope. Based on these results, a model has been proposed to explain the relationship between the lamellar structure and properties of PI composite film under different imidization stages, and the confinement of the thickness may be the most important factor for the formation of lamellar GS structure. © 2016 Wiley Periodicals, Inc. J. Appl. Polym. Sci. **2016**, *133*, 43575.

KEYWORDS: composites; films; graphene and fullerenes; nanotubes; polyimides; properties and characterization

Received 2 September 2015; accepted 23 February 2016
DOI: 10.1002/app.43575

INTRODUCTION

Compared with pure polymers, polymer-based nanocomposite materials possess much more excellent properties, which have attracted more and more attention in recent years. Polymer matrix could be endowed more and higher performances by incorporating a little of nanofillers, such as mechanical, electrical, thermal, and EMI shielding properties.[1–7] However, the property enhancement of the nanocomposite materials is related directly to the distribution of nanofillers in the polymer matrix, as well as interfacial interaction between the fillers and polymer matrix.[8] In recent research, the nanofillers such as functionalized graphene,[9] nanographene platelets,[10] and functionalized functionalized carbon nanotubes[11] can meet the requirements of both good dispersion and well interfacial interaction with polymer matrix for fabricating the composite materials in good performances.

Recently, in order to obtain higher performances of polymer-based composites, more investigations have been focused on the unique alignment of nanofillers in polymer matrix.[12–15] Dmitriy A. Dikin[16] prepared a free-standing carbon-based membrane material by the assembly of individual graphene oxide sheets, which had both macroscopic flexibility and stiffness. Kotov *et al.*[17] obtained a series of clay/polymer nacre-like artificial films with high flexibility and transparency via layer-by-layer assembly. Graphene fiber with highly ordered micrometer-sized structures had much more excellent properties.[18,19] Yao *et al.*[20] prepared nacre-like layered polymer/MTM hybrid films leading to a higher tensile strength. All these property improvements were related to the unique layered structure.[21–23]

However, researchers mostly focus on the influence of the layered orientation structure on the resin properties rather than pay attention to the formation process of this structure.[24] If the formation of the layered structure can be observed directly, it will play an important role on speculating the possible formation mechanism. Furthermore, with the well-dispersed nanofillers as the precondition, there are few reports about how the different orientation degrees affect the thermal, electrical, and mechanical properties of the nanocomposites. In this article, we

analyze the formation process of the lamellar structure by means of polyimide/graphene sheets (PI/GS) nanocomposites with different imidization degrees.

PI is considered as a typical high-performance engineering plastic with a widespread use of applications, because of its good chemical stability, excellent thermal, and mechanical properties. Recently, graphene-based nanofiller is introduced into the PI matrix due to its unique mechanical and thermal properties for fabricating PI-based nanocomposites with superior performances. Herein, we prepared PI/GS nanocomposites with different orientation degrees of graphene by controlling imidization degrees of PI, and the orientation process could be directly observed by means of scanning electron microscope (SEM). Moreover, the effect of GS layered structure on the thermal, electrical, and mechanical properties of the composite films during different imidization stage was also investigated. Finally, we also speculated the formation mechanism and pointed out the key factor of forming this layered structure.

EXPERIMENTAL

Materials

Natural graphite powder (325 mesh) was obtained from Qingdao Huatai Lubricant Sealing S&T Co. Ltd. Poly (amic acid) (PAA), the precursor of PI, was purchased from Shanghai Tonghao Industry & trade development Co. Ltd, and the solid content of the pristine PAA solution was 25%. N,N-Dimethylacetamide (DMAc), 37% HCl, 98% H_2SO_4, 30% H_2O_2, $KMnO_4$ and $NaNO_3$ were supplied by Sinopharm Chemical Reagent Co. Ltd. All reactants were analytical purity and used as received.

Preparation of Graphene Oxide Aqueous Solution and Graphite Oxide (GO)/DMAc Suspension

GO was synthesized based on a modified Hummers method as described elsewhere.[25] Then, the products were respectively three times washed with 5% HCl aqueous solution and DI water, and finally the GO aqueous solution was obtained. GO/DMAc suspension was prepared by utilizing a novel solvent-exchanged method. First, the GO aqueous solution was sonicated for 0.5 h and centrifuged at 16,000 rpm for 10 min to remove the DI water, and then a certain amount of DMAc was gradually added to replace DI water,. In this process, GO was kept in a solution state all the time instead of drying to avoid the damage on its structure. Then, the GO/DMAc dispersion was obtained with GO uniformly dispersed.

Preparation of PI and PI/GS Nanocomposites

Pure PI and PI/GS nanocomposite films were fabricated by conventional solution casting and subsequent thermal imidization method. First, the viscous pristine PAA solution was diluted by DMAc or GO/DMAc (2 mg/mL) suspension. The PAA and 1 wt % PAA/GO solutions were obtained by mixing 4 g pristine PAA solution with 5 mL DMAc and 5 mL GO/DMAc suspension, respectively.

In the next step, all the film specimens were first dried in a dry air-flowing oven at 60 C for 4 h to remove most of the solvent, and then, the cast films were thermally imidized via three different procedures, respectively: (1) heating from 60 °C up to 150 °C at a rate of 5 °C min^{-1} and staying for 1 h; (2) heating from 60 °C up to 250 °C at a rate of 5 °C min^{-1} and staying for 1 h; and (3) heating from 60 °C up to 250 °C and staying for 1 h, then gradually increasing to 350 °C and staying for 30 min at a rate of 5 °C min^{-1}. During the above thermal imidization process, the GO sheets could be partially *in situ* reduced to GS,[26] thus, the PI/GS nanocomposite films were obtained directly. For convenience, the corresponding samples were designated as PI/GS-60, PI/GS-150, PI/GS-250, and PI/GS-350, respectively.

Characterization

Fourier transform infrared (FTIR) spectra was recorded on a spectrometer (Nicolet Nexu) using the ATR mode to characterize and confirm the chemical structure of pure PI and PI/GS nanocomposite films. The morphology of the samples was observed by field SEM (FEI Sirion 200) with an acceleration voltage of 10 kV. The thermal stability was performed by thermogravimetric analysis (Perkin-Elmer Pyris 1) under nitrogen and air atmosphere, respectively, with each sample was tested for three times, and all the tests were run from 50 to 700 °C at a heating rate of 10 °C min^{-1}. The volume electrical conductivity was measured using a four-point probe resistivity measurement system (RST-9), all the samples were tested for three times and finally averaged. The tensile tests were used to obtain the stress–strain curves by universal testing machine (model CMT 4204; SANS Test, GB13022-91) in order to characterize the mechanical property with a stretch speeding of 5 mm min^{-1}. Three tests were repeated for each sample, and the values were averaged as the final result.

RESULTS AND DISCUSSION

GO is synthesized via a modified Hummers method and the micro-structure and morphology are shown in Figure 1(a). The Raman spectra of GO sheet shows the G peak at ~1600 $cm^{-1}$and a D peak at ~1350 cm^{-1}, indicative of the complete transformation from natural graphite to GO sheet. And the SEM images of GO shown in Figure 1(b) offer the evidence of peeled-off GO sheet directly.

A stepwise increase of temperature is necessary for the high quality of the PI nanocomposite film, and the formation process of the PI films is divided into three stages: (1) solution casting stage, (2) drying stage, and (3) thermal imidization stage. The critical temperatures are 150 and 200 °C where the conversion rate is the fastest and conversion achieves 90%, respectively. Finally, the imidization is fully completed at the temperature of 350 °C.[27] With this in mind, we choose 60 °C (the drying stage), 150 °C (the fastest imidization stage), 250 °C (the almost finished imidization stage), and 350 °C (the fully completed imidization stage) as the drying temperatures, respectively.

Figure 2 displays the appearances of the pure PI and PI/GS nanocomposite films under different drying temperatures. Pure PI film shows a light yellow color and it turns brown by the addition of GO (see Figure 2). Along with the growth of the drying temperature from 60 to 350 °C, pure PI film color gradually changes to dark yellow, and the PI/GS composite film turns to black finally. Yang *et al.*[28] reported that GO began to be reduced at 200 °C, and it shows a larger reaction degree at

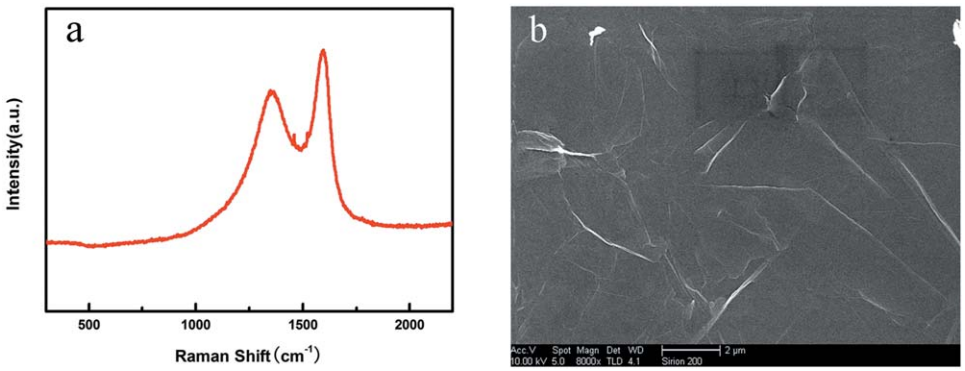

Figure 1. (a) Raman spectrum of GO sheet and (b) SEM images of GO sheet. [Color figure can be viewed in the online issue, which is available at wileyonlinelibrary.com.]

an increased temperatures. Thus, GO was gradually reduced to GS during the drying process. Then, the PI/GS nanocomposite film was obtained after the drying process. Meanwhile, all the PI/GS films present homogeneous appearances by visual inspection, indicating the GS was well dispersed in the PI matrix.

This could be contributed to the solvent-exchanged method that GO was well dispersed in DMAc. On one hand, DMAc is a strongly polar solvent which is capable of combination with the polar groups in GO sheets. On the another hand, the DMAc has the potential sites that can form hydrogen bonding with the PAA chains. Therefore, GO can disperse uniformly in PI because of its good compatibility with PI matrix.

IR Characterization

FTIR spectroscopy is utilized to characterize the imidization process of poly (amic acid) in PI/GS films. As shown in Figure 3, PAA shows the characteristic peaks[29] at 1660, 1607, 1545, and 1406 cm^{-1}. As the increase of the drying temperature, these absorption bands gradually weaken and finally disappear. Meanwhile, the absorption bands at 1776, 1726, and 1373 cm^{-1} are ascribed to PI and their intensities exhibit an upward trend with the growth of drying temperature. This result indicates that the PI/GS film achieves higher imidization degree at a higher drying temperature. In addition, the absorption peak at 1500 cm^{-1} is assigned to the ring stretching mode of the benzene in both PAA and PI. To further monitor the imidization process of PI/GS films, the characteristic absorption at 1500 cm^{-1} is chosen as reference. The relative absorbance intensity (A1373 cm^{-1}/A1500 cm^{-1}), as a representative of the imidization degree, is plotted as a function of drying temperature, as shown in the inset in Figure 3. It can be found that the imidization degree increases rapidly at the beginning of the rising drying temperature, then it varies very slowly after the temperature is higher than 200 °C. These above results are all consistent with that reported in literatures.[27]

Morphological Observation

SEM is used to observe the distribution of GS at different imidization degrees. As shown in Figure 4(a), GS presents a random distribution in the PI matrix and little or no imidization happens at a drying temperature of 60 °C. However, as the drying temperature gradually increasing to 150 °C, the GS layered structures begin to form only within some small regions. Once the drying temperature reaches up to 250 °C, GS are oriented along the direction of the film surface, so that the PI/GS films present obviously lamellar structures, as shown in Figure 4(c,d). All these results suggest that PI/GS nanocomposite films with

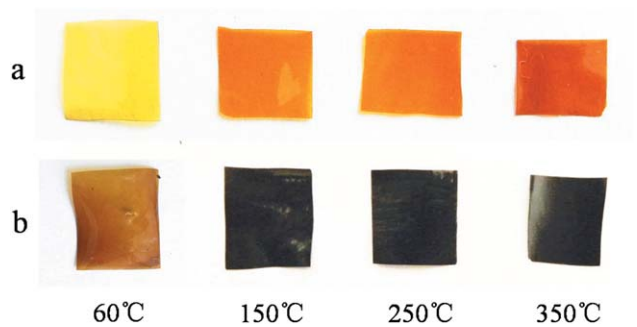

Figure 2. Digital photos of pure PI films (a) and PI/GS composite films (b) at different drying temperatures, all samples were treated at 60, 150, 250, and 350 °C, respectively. [Color figure can be viewed in the online issue, which is available at wileyonlinelibrary.com.]

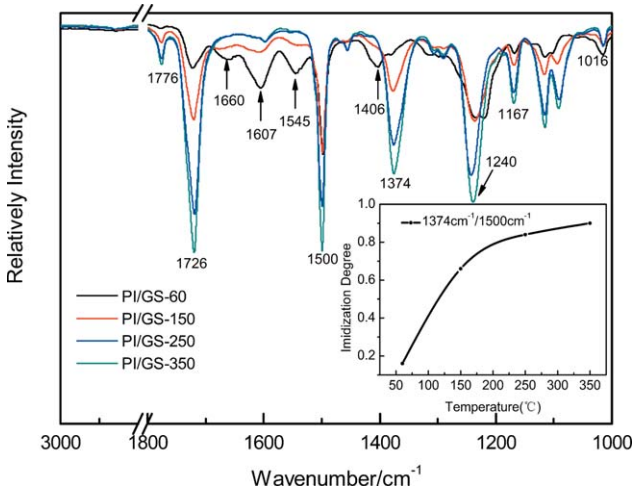

Figure 3. FTIR spectra of the imidization process of PI/GS nanocomposite film. The inset: Imidization degrees of PI/GS films under different drying temperatures. [Color figure can be viewed in the online issue, which is available at wileyonlinelibrary.com.]

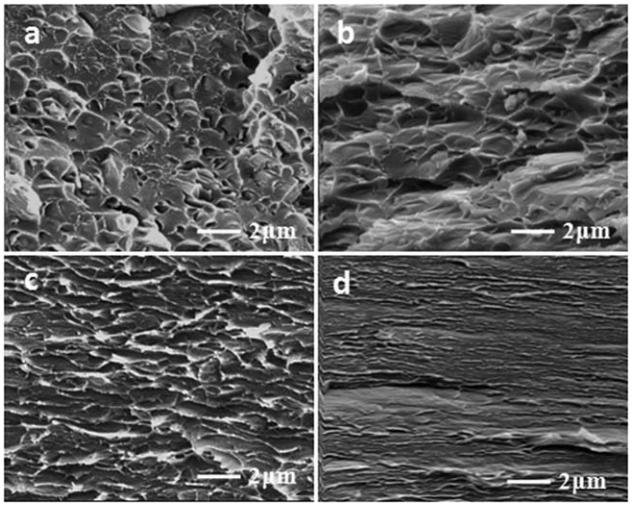

Figure 4. SEM micrographs of the cross-section surfaces of PI/GS films: (a) PI/GS-60, (b) PI/GS-150, (c) PI/GS-250, and (d) PI/GS-350.

different GS orientation degree can be prepared by controlling the imidization degree of PI.

Thermal Properties

Based on the different orientation distribution of GS in different imidization stages, we investigated its effect on thermal performances of PI films. Figure 5 shows the thermal decomposition process of pure PI film and PI/GS nanocomposite films at different imidization stages in N_2 atmosphere, respectively, and the degradation temperatures at 5 and 10 wt % mass loss ($T_{-5\%}$ and $T_{-10\%}$) is shown in Figure 6. It is obviously seen that the thermal stability of pure PI film increases gradually along with the improvement of the imidization degree (the increasing drying temperatures). For example, $T_{-5\%}$ of pure PI is raised from 154.3 to 582.4 °C as the drying temperature changes from 60 to 350 °C. The increasing trend of the thermal property is nearly consistent with the increasing imidization degree of pure PI film. This is mainly because the polyamic acid chains gradually convert into more rigid PI chains with the increase of imidization degree.

PI/GS nanocomposite film also shows the similar change tendency with the pure PI film, that the higher imidization degree results in the better thermal property. In addition, as shown in Figure 5, compared with the pure PI film, the thermal stability of the PI/GS nanocomposite film has been improved, as well as the $T_{-5\%}$ and $T_{-10\%}$ of PI/GS film as shown as in Figure 6. Moreover, the T_{max} of the thermal degradation of pure PI and PI/GS in N_2 atmosphere is summarized in Table I. It is obvious shown that the thermo-oxidative degradation of the samples occurs two distinct steps when the samples were dried at lower temperatures. The T_{max1} is shifted to higher values with the drying temperature increasing and eliminated at 350 °C. Besides, the T_{max2} of all the PI/GS samples are higher than that of the pure PI. All the results show the addition of GS has a better influence on the thermal property of the PI/GS composite film.

Table I. T_{max} of Pure PI and PI/GS Films in N_2 Atmosphere

Sample	T_{max1}	T_{max2}
Pure PI-60	162.0	609.9
Pure PI-150	217.9	611.6
Pure PI-250	305.9	615.8
Pure PI-350	—	629.1
PI/GS-60	167.1	630.9
PI/GS-150	213.9	621.6
PI/GS-250	303.8	621.9
PI/GS-350	—	629.2

Furthermore, the improvement of the thermal stability of the PI/GS nanocomposite film at the higher imidization degree is much larger than that at lower imidization degree, which is ascribed to the lamellar GS structure. The lamellar structure begins to form at 150 °C, where is a critical temperature with the fastest rate of imidization. Higher imidization degree promotes GS to form a layered structure paralleled to the surface, thus, more stable thermal properties are introduced into the system. Thus, in addition to the good compatibility, the lamellar alignment structure is also the key to improve the thermal property.

Besides, the thermal degradation process of pure PI and PI/GS films in an air atmosphere also presents the similar trend as that in N_2 atmosphere, as shown in Figure 7. Furthermore, the PI/GS film has much higher $T_{-5\%}$ and $T_{-10\%}$ than that of the pure PI films in air atmosphere compared with that in N_2

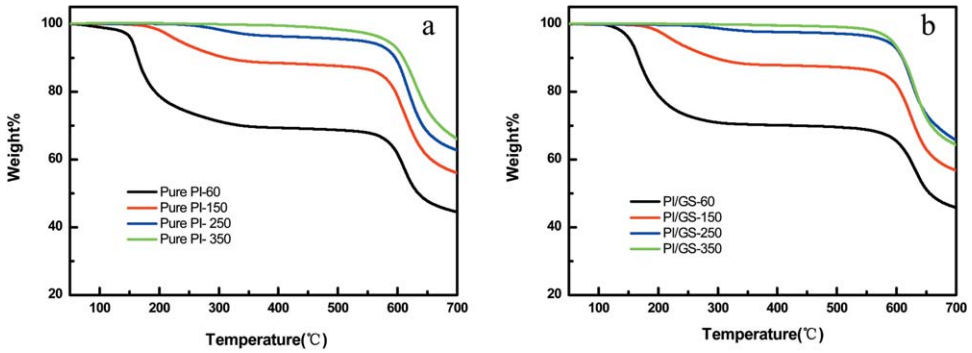

Figure 5. Thermogravimetric analysis (TGA) curves of the pure PI (a) and PI/GS (b) films at different imidization stages in N_2 atmosphere, respectively. [Color figure can be viewed in the online issue, which is available at wileyonlinelibrary.com.]

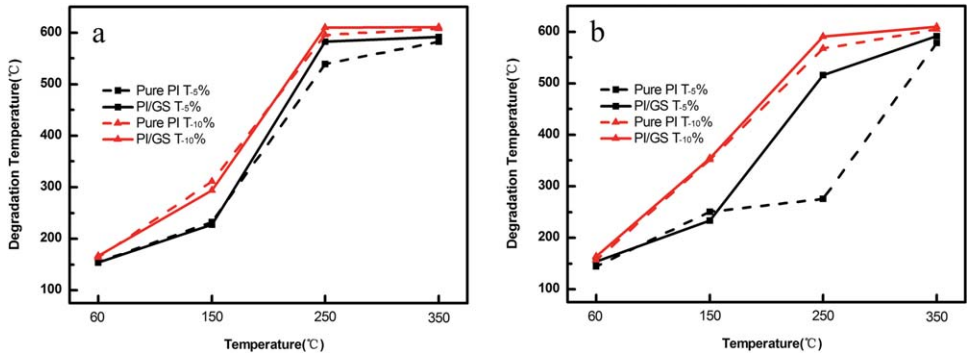

Figure 6. $T_{-5\%}$ and $T_{-10\%}$ of pure PI and PI/GS in N_2 (a) and air (b) atmosphere, respectively. [Color figure can be viewed in the online issue, which is available at wileyonlinelibrary.com.]

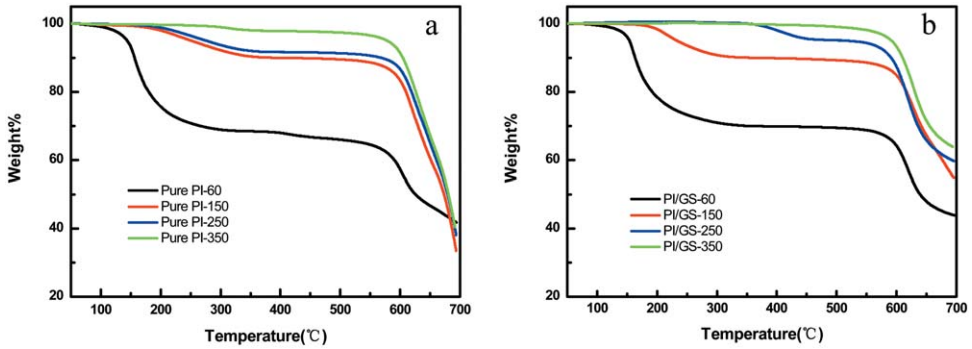

Figure 7. Thermogravimetric analysis (TGA) curves of the pure PI (a) and PI/GS (b) films at different imidization stages in air atmosphere, respectively. [Color figure can be viewed in the online issue, which is available at wileyonlinelibrary.com.]

atmosphere. The oxygen in the air atmosphere has participated into the decomposition reaction, thereby accelerating the decomposition process of the films. The lamellar structure of PI/GS films with a better performance has reduced this accelerating action.

Electrical Conductivity

Pure PI is an insulating material with an electrical conductivity of $\sim 10^{-15}$ S cm^{-1}. The addition of GS significantly improves the electrical conductivity of PI/GS composite film, as shown in Figure 8. For example, PI/GS-60 film has an electrical conductivity of 6.4×10^{-11} S cm^{-1}, which is a ~4 order of magnitude higher than that of pure PI film. What's more, the electrical conductivity increases with growth of the drying temperature. As the drying temperature increases to 350 °C, the electrical conductivity of PI/GS film reaches up to 2.3×10^{-7} S cm^{-1}, increased by 8 order of magnitude as compared with pure PI

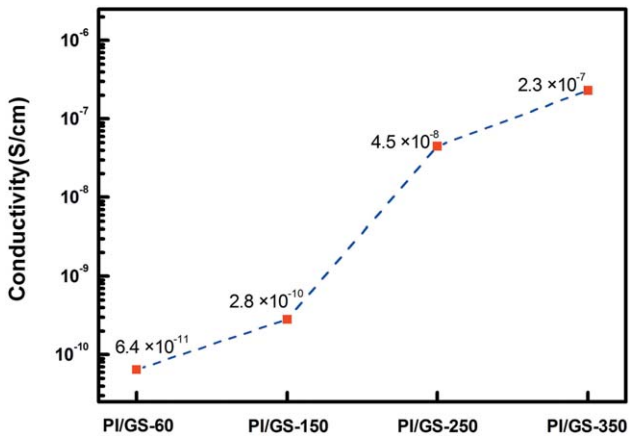

Figure 8. Electrical conductivity of PI/GS nanocomposite films at different drying temperatures. [Color figure can be viewed in the online issue, which is available at wileyonlinelibrary.com.]

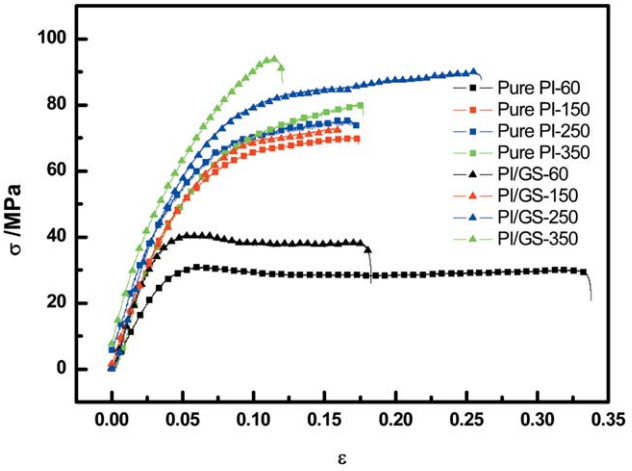

Figure 9. Typical stress–strain curves of pure PI and PI/GS nanocomposite films at different drying temperatures. [Color figure can be viewed in the online issue, which is available at wileyonlinelibrary.com.]

Table II. The Tensile Strength, Elastic Modulus, and Elongation at Break of Pure PI and PI/GS Films, Respectively

Samples	Tensile strength (MPa)	Elastic modulus (MPa)	Elongation at break (%)
Pure PI-60	30.8	844.5	33.8
Pure PI-150	70.0	1193.0	17.4
Pure PI-250	75.2	1277.9	17.2
Pure PI-350	80.1	1208.9	17.7
PI/GS-60	40.4	1320.6	18.3
PI/GS-150	72.9	1091.3	16.2
PI/GS-250	89.9	1386.4	26.0
PI/GS-350	94.0	1286.2	12.1

film. The above results can be attributed to two reasons: First, the reduction degree of GO sheets increases with the increasing drying temperatures. Second, the formation of lamellar GS structure leads to a better conductive network at higher temperature.

Mechanical Properties

Figure 9 shows the typical stress–strain curves of pure PI and PI/GS nanocomposite films, and the corresponding data are collected in Table II. Because of the higher imidization degree, pure PI and the PI/GS composite films show improved tensile strength at an increased drying temperature, as shown in Table II. For example, the tensile strength increases from 30.8 and 40.4 MPa of pure PI-60 and PI/GS-60 to 80.1 and 94.0 MPa of pure PI-350 and PI/GS-350, respectively. It is noteworthy that the PI/GS composites show enhanced tensile strength as compared with pure PI film, which could be attributed to the incorporation of GS into PI matrix. In Addition, compared with the pure PI samples, the addition of rigid GS fillers leads to a little reduction on elongation at break for the PI/GS composites, while the tensile strength and elastic modulus of the composites are significantly enhanced, which indicates the composites owing better strength and higher mechanical property. This result is consistent with the influence of the GS on the thermal and electrical properties of PI/GS composite film. From the above mentioned results, the distribution of GS plays an important role in improving the thermal property and mechanical property of the nanocomposite film.

Based on these results, the formation process of the lamellar GS structure within PI matrix can be explained by a simplified schematic diagram, as illustrated in Figure 10. The dilute PAA solution includes plenty of solvent and the well dispersed GO sheets [Figure 10(a)]. The solvent molecules begin to volatile and the thickness of the film becomes thinner remarkably as the increase of drying temperature (as illustrated in Figure 10). In the case of the drying temperature of 60 C, there is still enough space to allow the GO sheets freely dispersed [Figure 10(b)]. When the drying temperature increases to 150 C, GO sheets is reduced to GS partially, and it must be scattered at smaller spaces that might be preferentially aligned along the surface of the nanocomposite film. As the drying temperature growing, the evaporation of the left solvent promotes the imidization degree, along with the film thickness declining strongly, which even dropping to half of that at 60 C, as displayed in Figure 11. In this case, the GS are compelled to orient along the film surface to be able to save the space in thin films. Therefore, the property of the nanocomposite film is significantly improved with the increasing imidization degree and the orientation of GS.

In addition, the GS lamellar structure occurs at higher drying temperatures while less solvent is evaporated at this stage, which

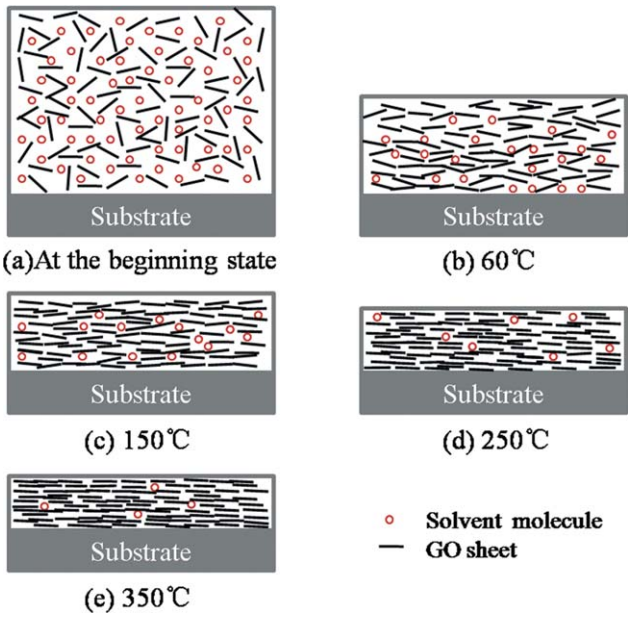

Figure 10. Scheme showing the possible orientation mechanism of GS in PI/GS nanocomposite films during the drying temperature increasing process. [Color figure can be viewed in the online issue, which is available at wileyonlinelibrary.com.]

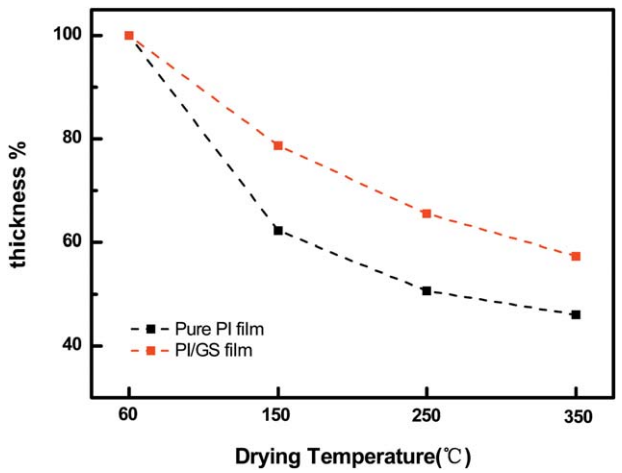

Figure 11. Change of thickness at different drying temperatures. [Color figure can be viewed in the online issue, which is available at wileyonlinelibrary.com.]

indicating the evaporated solvent is unnecessary for forming this lamellar structure. This result is different from the mechanism that solvent evaporation induces the orientation reported in the literature.[30] The thickness of the films has reduced significantly, which forces the GS to be dispersed as a layered structure that the most space-saving arrangement. Thus, we speculate the thickness confinement may be the most important factor rather than the solvent evaporation for the well oriented GS in the nanocomposite film.

CONCLUSIONS

We obtain a uniformly dispersed GO/DMAc suspension via a solvent-exchanged method and mixes with the pristine PAA solution subsequently. Then, the mixed solutions are imidized at different temperatures with the GO sheets reducing to GS, and the imidization degree of the films becomes higher due to the drying temperature increasing. The excellent thermal, electrical, and mechanical performances of PI/GS nanocomposite film are ascribed to the higher imidization degree and the GS lamellar structure. Besides, we observe the formation process of the lamellar structure directly by SEM, GS are gradually paralleled to the film surface as the drying temperature increasing. Finally we propose a schematic diagram to illustrate the formation process of the lamellar structure and speculate the restriction of the thickness is the most important factor to form this lamellar structure.

ACKNOWLEDGMENTS

The authors are grateful to the support of National Natural Science Foundation of China (No. 51303182, 21204090, and 51402002).

REFERENCES

1. Stankovich, S.; Dikin, D. A.; Dommett, G. H.; Kohlhaas, K. M.; Zimney, E. J.; Stach, E. A.; Piner, R. D.; Nguyen, S. T.; Ruoff, R. S. *Nature* **2006**, *442*, 282.
2. Li, C.; Shi, G. *Nanoscale* **2012**, *4*, 5549.
3. Wang, Y.; Chen, S.; Qiu, L.; Wang, K.; Wang, H.; Simon, G. P.; Li, D. *Adv. Funct. Mater.* **2015**, *25*, 126.
4. Sun, H.; You, X.; Deng, J.; Chen, X.; Yang, Z.; Ren, J.; Peng, H. *Adv. Mater.* **2014**, *26*, 2868.
5. Yao, H. B.; Ge, J.; Wang, C. F.; Wang, X.; Hu, W.; Zheng, Z. J.; Ni, Y.; Yu, S. H. *Adv. Mater.* **2013**, *25*, 6692.
6. Zhang, Y.; Huang, Y.; Zhang, T.; Chang, H.; Xiao, P.; Chen, H.; Huang, Z.; Chen, Y. *Adv. Mater.* **2015**, *27*, 2049.
7. Zhang, J.; Jiang, D. *Carbon* **2014**, *67*, 784.
8. Kuilla, T.; Bhadra, S.; Yao, D.; Kim, N. H.; Bose, S.; Lee, J. H. *Prog. Polym. Sci.* **2010**, *35*, 1350.
9. Cai, D.; Song, M. *J. Mater. Chem.* **2010**, *20*, 7906.
10. Jang, B. Z.; Zhamu, A. *J. Mater. Sci.* **2008**, *43*, 5092.
11. Song, K.; Zhang, Y.; Meng, J.; Green, E.; Tajaddod, N.; Li, H.; Minus, M. *Materials* **2013**, *6*, 2543.
12. Yao, H. B.; Ge, J.; Mao, L. B.; Yan, Y. X.; Yu, S. H. *Adv. Mater.* **2014**, *26*, 163.
13. Yang, X.; Zhu, J.; Qiu, L.; Li, D. *Adv. Mater.* **2011**, *23*, 2833.
14. Zhao, Q.; An, Q. F.; Liu, T.; Chen, J. T.; Chen, F.; Lee, K. R.; Gao, C. *J. Polym. Chem.* **2013**, *4*, 4298.
15. Liu, Y.; Wang, W.; Wang, Y.; Peng, X. *Nano Energy* **2014**, *7*, 25.
16. Dikin, D. A.; Stankovich, S.; Zimney, E. J.; Piner, R. D.; Dommett, G. H.; Evmenenko, G.; Nguyen, S. T.; Ruoff, R. S. *Nature* **2007**, *448*, 457.
17. Podsiadlo, P.; Kaushik, A. K.; Arruda, E. M.; Waas, A. M.; Shim, B. S.; Xu, J.; Nandivada, H.; Pumplin, B. G.; Lahann, J.; Ramamoorthy, A.; Kotov, N. A. *Science* **2007**, *318*, 80.
18. Xu, Z.; Sun, H.; Zhao, X.; Gao, C. *Adv. Mater.* **2013**, *25*, 188.
19. Xu, Z.; Liu, Z.; Sun, H.; Gao, C. *Adv. Mater.* **2013**, *25*, 3249.
20. Yao, H. B.; Tan, Z. H.; Fang, H. Y.; Yu, S. H. *Angew. Chem.* **2010**, *49*, 10127.
21. Shu, Y.; Yin, P.; Liang, B.; Wang, H.; Guo, L. *ACS Appl. Mater. Interfaces* **2014**, *6*, 15154.
22. Zhang, M.; Huang, L.; Chen, J.; Li, C.; Shi, G. *Adv. Mater.* **2014**, *26*, 7588.
23. Pham, V. H.; Dang, T. T.; Hur, S. H.; Kim, E. J.; Chung, J. S. *ACS Appl. Mater. Interfaces* **2012**, *4*, 2630.
24. Ha, H. W.; Choudhury, A.; Kamal, T.; Kim, D. H.; Park, S. Y. *ACS Appl. Mater. Interfaces* **2012**, *4*, 4623.
25. Zhang, H.; Xie, A.; Wang, C.; Wang, H.; Shen, Y.; Tian, X. *J. Mater. Chem. A* **2013**, *1*, 8547.
26. Chen, W.; Yan, L.; Bangal, P. R. *Carbon* **2010**, *48*, 1146.
27. Unsal, E.; Cakmak, M. *Macromolecules* **2013**, *46*, 8616.
28. Yang, D.; Velamakanni, A.; Bozoklu, G.; Park, S.; Stoller, M.; Piner, R. D.; Stankovich, S.; Jung, I.; Field, D. A.; Ventrice, C. A.; Ruoff, R. S. *Carbon* **2009**, *47*, 145.
29. Huang, T.; Lu, R.; Su, C.; Wang, H.; Guo, Z.; Liu, P.; Huang, Z.; Chen, H.; Li, T. *ACS Appl. Mater. Interfaces* **2012**, *4*, 2699.
30. Chen, D.; Zhu, H.; Liu, T. *ACS Appl. Mater. Interfaces* **2010**, *2*, 3702.